ACS Macro Letters

Letter

pubs.acs.org/macroletters

Theory of Anisotropic Diffusion of Entangled and Unentangled Polymers in Rod−Sphere Mixtures

Umi Yamamoto[†,∥] and Kenneth S. Schweizer*[,‡,§]

[†]Department of Physics, [‡]Departments of Materials Science and Chemistry, and [§]Frederick Seitz Materials Research Laboratory, University of Illinois, Urbana, Illinois 61801, United States

Supporting Information

ABSTRACT: We present a microscopic self-consistent theory for the long-time diffusion of infinitely thin rods in a hard sphere matrix based on the simultaneous dynamical treatment of topological uncrossability and finite excluded volume constraints. Distinctive regimes of coupled anisotropic longitudinal and transverse diffusion are predicted, and steric blocking of the latter leads to a tube-like localization transition largely controlled by the ratio of the sphere diameter to rod length and tube diameter. For entangled polymers, in a limited regime of strongly retarded dynamics a "doubly renormalized" reptation law is predicted where the confinement tube is compressed and longitudinal motion is partially blocked. At high sphere volume fractions, strong suppression of rod motion results in dynamic localization in the unentangled regime. The present advance provides a theoretical foundation to treat differential mobility effects and flexible chain dynamics in diverse polymer−particle mixtures.

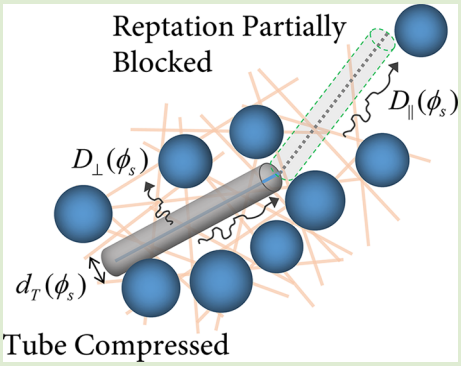

Understanding the unique slow dynamics of liquids of topologically entangled macromolecular objects is a fascinating problem relevant to polymer physics, cellular biology, and engineering materials.[1−4] For polymer fluids of linearly connected flexible chains or rigid rods this problem is commonly treated based on the reptation-tube model.[1,3,4] This phenomenological approach replaces, by assumption, the many-body dynamical consequences of polymer uncrossability and connectivity by an effectively static "tube" confinement field. The latter enforces transient transverse localization on an intrinsic mesoscopic length scale, the "tube diameter". Knowledge of the latter then immediately allows predictions to be made for long-time diffusion using scaling arguments and the assumption that anisotropic, curvilinear Brownian motion along the polymer contour (reptation) is the dominant motion.[4]

Entangled polymer dynamics must be a richer and far more complex problem in polymer−particle mixtures or "nanocomposites" due to the presence of additional length and time scales and finite excluded volume and geometric confinement, the fundamental understanding of which is in its infancy.[5−12] Impenetrable obstacles are expected to result in at least four *qualitatively* new physical effects: (i) the tube can tighten due to sphere-induced confinement, (ii) the reptation motion could be slowed down (or destroyed) due to enhanced frictional and/or geometric blocking effects, (iii) longitudinal and transverse diffusivities may become strongly coupled, and (iv) rigid polymers can literally localize. Recent experiments[6−10] and simulations[11] on chain polymer nanocomposites have just begun to address some of these issues. They find that the addition of spherical particles leads to a smaller apparent tube diameter[6,10] and slower center-of-mass (CM) diffusion.[7−9] However, even at zeroth order, no theoretical understanding exists due to the high difficulty of treating in a unified manner the consequences of topological uncrossability and excluded volume interactions. We believe progress requires the formulation of a tractable first-principles approach[12,13] based on merging concepts of polymer and liquid-state physics, which is the topic of this Letter.

Our starting point builds on two recent theoretical advances. The first is a microscopic self-consistent dynamic theory[13] for a structurally ideal fluid of nonrotating, topologically entangled, infinitely thin rods or "needles" of length L and dimensionless number density $\rho_r^* \equiv \rho_r L^3$. It successfully predicts the emergence of a confinement tube when $\rho_r^* > \rho_e^* \approx 10$, with diameter $d_{T,0} \propto 1/\rho_r^*$ when $\rho_r^* \gg \rho_e^*$, and quantitatively agrees with simulation for diffusion constants.[14] Second, this approach has very recently been generalized to mixtures of needles and immobile hard spheres (radius R, volume fraction $\phi_s \equiv 4\pi\rho_s R^3/3$) for the single question of *intermediate*-time transverse localization. On the basis of quenching longitudinal rod motion, tube compression is predicted, $d_T(\phi_s)/d_{T,0} \sim 1/(1 + a\phi_{\text{eff}})$, where $\phi_{\text{eff}} = \phi_s(d_{T,0}/2R)(L/2R) \propto \rho_s R L d_{T,0}$ and a is a numerical constant.[12] Using self-consistent primitive path and chain-to-needle mapping ideas,[15] this theory predicts tube diameters in good agreement with simulations.[11,16]

The second advance above addresses point (i) but is entirely inadequate for understanding long-time diffusion since the longitudinal transport (reptation) can be fundamentally altered by the new physics contained in points (ii)−(iv). This stands in

Received: November 7, 2014
Accepted: December 15, 2014
Published: December 22, 2014

 © 2014 American Chemical Society

qualitative contrast to pure polymer fluids where the reptation motion is "free" (unaffected by interneedle collisions) and decoupled from transverse motion. Here we develop a general dynamical theory for needle−sphere mixtures and implement it to study long-time diffusivity in the specific context of a spatially fixed array of hard spheres with a statistically random microstructure. The fixed sphere limit is the simplest fundamental starting point, in analogy with the classic analysis of the "prototype" problem of a single chain reptating in a fixed array of topological obstacles.[3,4] This limit is also *directly* relevant to real nanocomposites when particles are sufficiently large that they are effectively immobile on the polymer diffusion time scale.[8,9]

Physically, we expect many dynamical regimes exist as a consequence of the presence of multiple length-scale ratios and two qualitatively new collisional processes (see Figure 1): a

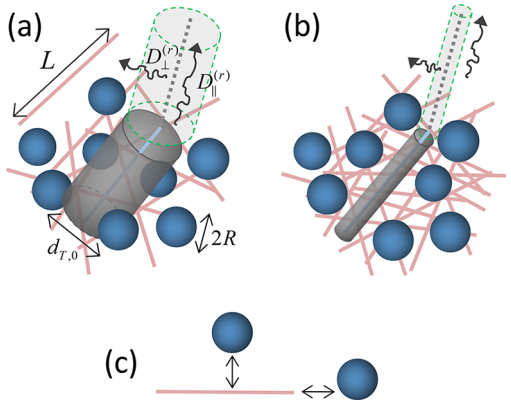

Figure 1. Schematics of a rod−sphere mixture showing characteristic length scales, anisotropic diffusion constants, different rod concentration regimes, and distinct collisions. (a) Low rod concentrations where the pure-needle tube diameter, $d_{T,0}$, is greater than the sphere diameter, $2R$. (b) High rod concentrations which involve less side-on rod−sphere collisions due to a "tight" tube where $d_{T,0} < 2R$. (c) Two types of rod−sphere collisions (side-on and end-on).

"side-on" collision that modifies only needle transverse motion and an "end-on" collision that simultaneously affects transverse and longitudinal motion in a correlated manner. The latter will be shown to result in a *qualitative* breakdown of pure-needle dynamics with longitudinal motion no longer free and self-consistently coupled to transverse motion. The distinct dynamical regimes are determined by the relative and absolute importance of rod−rod and rod−sphere collisions which are a rich function of ρ_r^*, particle size relative to the "bare" tube diameter, $2R/d_{T,0}$, aspect ratio, $\gamma \equiv L/2R$, and the mean geometric confinement scale, $\propto R\phi_s^{-1/3}$. We address in a unified manner all four physical aspects raised in the Introduction and answer the following questions. How does the pure fluid reptation-tube model break down? Can the reptation-tube framework be "renormalized" in certain regimes to describe nanocomposites? Do entirely new phenomena emerge? How do the multiple length scales inherent to the rod−sphere mixture control polymer diffusion?

We have constructed a general two-component theory for mobile needles and particles based on effective Smoluchowski equations that include exactly at the two-body level rod topological uncrossability and rod−sphere excluded volume constraints via collision "T-operators";[12−14,17] higher-order dynamical correlations are accounted for through infinite order via a self-consistent closure. As described in the SM,[18] for immobile spheres and random liquid structure, the self-consistent equations for the rod effective diffusion tensor, $\hat{D}^{(r)}(\vec{u}_1)$, become

$$\hat{D}^{(r)-1} = \hat{D}_0^{(r)-1} - \sum_{\alpha=r,s} \rho_\alpha \int D\vec{r} g_{r\alpha}(\vec{r}) \vec{T}^{(r\alpha)}(\vec{r}) \times [\Omega_e^{(r\alpha)\dagger}(z \to 0)]^{-1} \vec{T}^{(r\alpha)}(\vec{r}) \quad (1)$$

Here, $\hat{D}_0^{(r)}$ is the "bare" rod diffusion tensor; $\vec{u}_i$ is the orientation vector of particle i; $\alpha = r,s$ indicates rod and sphere; ρ_α is the number density of species α; $\vec{r}$ is the interparticle CM separation vector; $g_{r\alpha}$ is the pair correlation function (here random); $D\vec{r} = d\vec{r}d\vec{u}_2/(4\pi)$ for rods and $D\vec{r} = d\vec{r}$ otherwise; $\Omega_e^{(r\alpha)\dagger}(z \to 0) = (\vec{\nabla} + \vec{T}^{(r\alpha)})\cdot[\hat{D}^{(r)} + \hat{D}^{(\alpha)}]\cdot\vec{\nabla}$ is the adjoint of the long-time effective Smoluchowski operator; and $\vec{T}^{(r\alpha)}$ is the T-operator. The anisotropic rod diffusion tensor is $\hat{D}^{(r)}(\vec{u}_1) = D_\parallel^{(r)}\vec{u}_1\vec{u}_1^T + D_\perp^{(r)}(1 - \vec{u}_1\vec{u}^T)$, where $D_\perp^{(r)}$ ($D_\parallel^{(r)}$) is the rod transverse (longitudinal) diffusion constant and $D^{(s)} = 0$ for fixed spheres.

Two coupled self-consistent equations for the needle diffusion constants can be derived from eq 1[18]

$$\frac{D_\perp^{(r)}}{D_{\perp,0}^{(r)}} = 1 - \rho_r^* \varepsilon F_\perp^{(rr)}(\varepsilon^2) - \phi_s F_\perp^{(rs)}(\varepsilon;\gamma),$$
$$\frac{D_\parallel^{(r)}}{D_{\parallel,0}^{(r)}} = 1 - \phi_s F_\parallel^{(rs)}(\varepsilon;\gamma) \quad (2)$$

where $\varepsilon \equiv (D_\perp^{(r)}/D_\parallel^{(r)})^{1/2}$ quantifies diffusion anisotropy and the rod−rod and rod−sphere collision contributions are represented by $F_\perp^{(rr)}$ (see ref 13), $F_\perp^{(rs)}$, and $F_\parallel^{(rs)}$[18]

$$F_\perp^{(rs)}(\varepsilon;\gamma) \equiv -\frac{3}{2}(1+\gamma)^3\varepsilon^2 \sum_{n=0}^{\infty} \frac{(4n+1)}{\zeta_0}\frac{q_{2n}(\zeta_0)}{q'_{2n}(\zeta_0)} \times c_{2n}(0)c_{2n}\left(\frac{\gamma}{1+\gamma}\right) \quad (3a)$$

$$F_\parallel^{(rs)}(\varepsilon;\gamma) \equiv -3(1+\gamma)^3\frac{1}{\zeta_0}\frac{q_1(\zeta_0)}{q'_1(\zeta_0)}c_1\left(\frac{\gamma}{1+\gamma}\right) \quad (3b)$$

In eqs 3a and 3b, $\zeta_0 \equiv (1+\gamma)\varepsilon/|(1+\gamma)^2\varepsilon^2 - 1|^{1/2}$, $q_n(x)$ is a specific Legendre function of the second kind,[18,19] $c_{2n}(x) \equiv \int_0^x d\mu P_{2n}(\mu) + \int_x^1 d\mu(1-\mu^2)^{1/2}P_{2n}(\mu)$ and $c_{2n+1}(x) \equiv \int_x^1 d\mu (\mu - x)P_{2n+1}(\mu)$ involve Legendre polynomial of the first kind, $P_n(x)$. Equation 2 explicitly demonstrates longitudinal needle motion is only affected by rod−sphere collisions. Analytic forms of eqs 3a and 3b in the $\gamma \gg 1$ and $\varepsilon(1+\gamma) \ll 1$ limit can be derived[18] as $F_\perp^{(rs)} \propto \gamma^2\varepsilon$ and $F_\parallel^{(rs)} \propto \gamma^0/\varepsilon$, illustrating the sharp contrast between how the aspect ratio and diffusivity ratio determine the dynamical consequences of head-on and side-on collisions.

Figure 2 presents representative calculations of the transverse and longitudinal diffusion constants as a function of sphere volume fraction for a low and high aspect ratio; rod density ranges from the dilute to heavily entangled regimes. Both diffusivities monotonically decrease with ϕ_s at a rate that grows with rod density (more topological entanglements, tighter pure-needle-fluid tube) and aspect ratio. Both the opposite curvatures of the two diffusion constant curves and the more rapid suppression of transverse motion with sphere loading are

dx.doi.org/10.1021/mz500708z | ACS Macro Lett. 2015, 4, 53−57

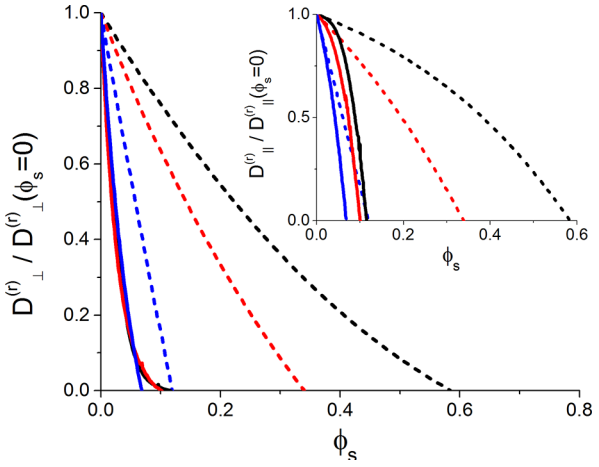

Figure 2. Rod transverse diffusion constant (normalized by its pure-polymer-fluid value) as a function of sphere volume fraction for two aspect ratios, γ = 1 (dash) and 8 (solid), and three reduced rod number densities ρ_r^* = 0 (black), 20 (red), 80 (blue); the latter two correspond to $2R/d_{T,0}$ = 2.42, 10.8 for γ = 1, and 0.302, 1.35 for γ = 8, respectively. (Inset) Same plot for the reduced longitudinal diffusion constant.

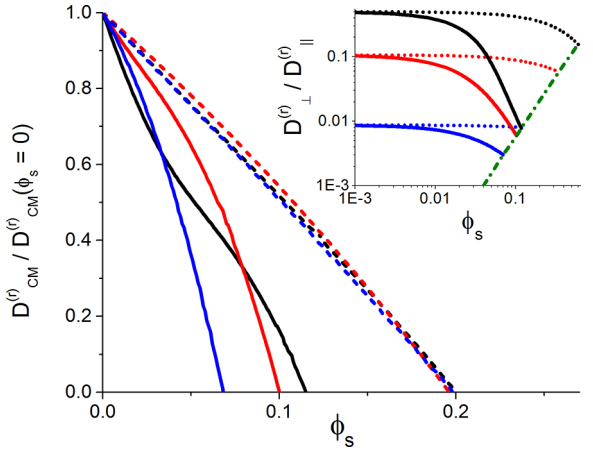

Figure 3. Reduced rod CM diffusion constant vs sphere volume fraction corresponding to Figure 2 for γ = 1 (dash) and 8 (solid) using the same color codes and line types. To clearly illustrate the near collapse in shape, the γ = 1 results are shown with the x-axis rescaled by a factor of ~0.331, 0.579, and 1.68 for ρ_r^* = 0, 20, and 80, respectively. (Inset) Ratio of the transverse and longitudinal diffusion constants vs sphere volume fraction. The green dash-dot line indicates a slope of 2.

direct consequences of the extended needle shape where more side-on versus end-on collisions occur. This effect is more pronounced for larger aspect ratios and/or smaller rod concentrations or more generally larger values of $(d_{T,0}/2R)(L/2R)$, for which the transient transverse localization (tube compression) effect is enhanced.[12] In contrast, the two diffusivities decrease in a relatively symmetric and strongly coupled manner for highly entangled rods. The physical reason is that side-on collisions are now restricted by the tight pure-needle tube, so end-on collisions "blocking" longitudinal motion, which simultaneously affect and couple the two diffusivities, dominate. These two physically distinct situations are illustrated in Figure 1. As a generic consequence of the fixed sphere condition and polymer rigidity, a simultaneous localization of longitudinal and transverse motion is predicted at a critical volume fraction, ϕ_c.

Figure 3 studies the consequences of anisotropic diffusion in two ways. First, the inset shows that the diffusion constant ratio is always reduced (enhanced anisotropy) with increasing sphere loading, rod number density, and aspect ratio. However, its growth with ϕ_s weakens as more topological entanglements are present (higher ρ_r^*) and for shorter rods (smaller $L/2R$), corresponding to the $2R/d_{T,0} \gg 1$ regime where the end-on "blocking" effect becomes significant. The diffusivity ratio tends to a finite value as the localization transition is approached, approximately satisfying the scaling law[18] $D_\perp^{(r)}/D_\parallel^{(r)} \propto \phi_c^2$.

The CM diffusion constant, $D_{CM}^{(r)} = (2D_\perp^{(r)} + D_\parallel^{(r)})/3$, is experimentally measurable. For the low-aspect-ratio "tight" tube cases ($d_{T,0} \ll 2R$), Figure 3 shows that $D_{CM}^{(r)}$ decreases roughly linearly with ϕ_s, and different rod density systems nearly collapse (not shown) if the horizontal axis is normalized with respect to ϕ_c as a result of the relatively weak dependence of diffusional anisotropy on ϕ_s (Figure 3, inset). In contrast, for large aspect ratios, $D_{CM}^{(r)}$ is a more complicated, nonlinear function of sphere loading. These features are strongest in the tracer limit and reflect a nonuniversal competition between topological entanglements and rod−sphere collisions. Specifically, at low ρ_r^* and/or large γ (where $d_{T,0} \gg 2R$) the CM motion is controlled mainly by side-on rod−sphere collisions which only suppress transverse diffusion. However, at large ρ_r^* and/or small γ (where $d_{T,0} \ll 2R$), needles have less space for transverse dynamical fluctuation, and it becomes harder for them to avoid or "go around" obstacles. As a consequence, the suppression of $D_{CM}^{(r)}$ is primarily caused by the longitudinal motion becoming partially blocked, an effect we call "tube capping". For dilute rods, the general form of the slowdown of D_{CM} due to sphere crowding is in qualitative agreement[20] with existing simulation studies in 3-dimensions.[22]

The above results suggest a physical picture whereby the rich dynamical consequences of sphere excluded volume can be understood in terms of two effects with distinct dependences on ϕ_s, aspect ratio, and rod density: tube compression due to sphere-induced lateral confinement and blocking of reptation. The latter generally dominates if $d_{T,0} < 2R$ where rod−sphere side-on collisions are less likely than end-on collisions. The dynamics of unentangled rods is simpler, and diffusion anisotropy is mainly controlled by the lateral confinement effect.

We now investigate whether a deeply modified "renormalized" form of reptation might be relevant in entangled systems. In the pure-needle fluid the tube diameter and diffusion constants are related via the scaling law,[3,12] $D_\perp^{(r)}/D_\parallel^{(r)} \propto (d_{T,0}/L)^2 \propto (1/\rho_r^*)^2$ with $D_\parallel^{(r)} = D_{\parallel,0}^{(r)}$ for $\rho_r^* \gg 1$ (in practice >40), but there is no guarantee such a motional mechanism and scaling relation exist in rod−sphere mixtures. However, we can derive[18] from eq 2 that the form of the above classic relation holds if $\rho_r^* \gg 1$ and $D_\perp^{(r)}/D_\parallel^{(r)} \ll (1/\gamma)^2$, thereby obtaining

$$D_\perp^{(r)} = D_\parallel^{(r)}(\phi_s)\left[\frac{d_T(\phi_{\text{eff}})}{L}\right]^2 = D_{\perp,\text{pure rod}}^{(r)}\left[\frac{d_T(\phi_{\text{eff}})}{d_{T,0}}\right]^2\left(\frac{D_\parallel^{(r)}(\phi_s)}{D_{\parallel,0}^{(r)}}\right) \quad (4)$$

where $d_T(\phi_s)$ was given above and $a \equiv 1.93$. While eq 4 is not predictive unless one of the diffusion constants is known, it establishes the physical picture of an entangled rod diffusing via an *effective* reptative motion where two (coupled) sphere-induced renormalizations enter: the tube is compressed *and* longitudinal motion is slowed. The inequalities that underlie

dx.doi.org/10.1021/mz500708z | ACS Macro Lett. 2015, 4, 53−57

the applicability of eq 4 imply $L^2/D_{\parallel}^{(r)} \ll (2R)^2/D_{\perp}^{(r)}$, which corresponds to a time-scale separation that assures renormalized reptation is "fast enough" on the sphere length scale. Whether these conditions are achieved in a specific mixture is subtle given the localization transition occurs at sufficiently high ϕ_s due to complete blocking of reptation.

Figure 4 presents calculations of the transverse diffusivity as a function of rod concentration based on eqs 3 and 4. The pure-

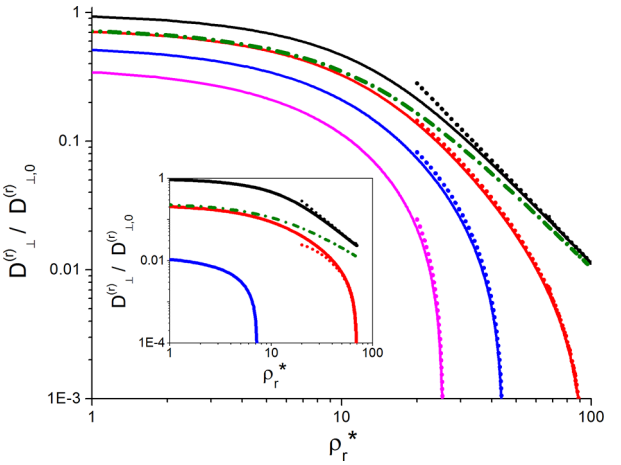

Figure 4. Dimensionless transverse diffusion constant vs reduced rod number density for $\gamma = 1$ and $\phi_s = 0$ (black), 0.1 (red), 0.2 (blue), and 0.3 (pink). Solid curves follow from eq 2, and the corresponding dotted curves indicate the renormalized reptation relation eq 4. The green dash-dot curve shows an example of a "virtual" calculation where the longitudinal diffusivity is unchanged by sphere addition. (Inset) Same plot for $\gamma = 4$.

needle reptation scaling law continuously fails as sphere concentration grows. The rod transverse diffusivity agrees well with eq 4 beginning in the lightly entangled regime for relatively small aspect ratios. However, if γ and ϕ_s are large, rods localize before topological entanglements emerge. On the other hand, eq 4 is generically satisfied in the $\rho_r^* \gg 1$ regime if the system is not close to the localization transition. This point is demonstrated in Figure 4 by performing a "virtual" calculation where the free reptation value is enforced by hand for the longitudinal diffusion constant $(D_{\parallel}^{(r)}(\phi_s) \rightarrow D_{\parallel,0}^{(r)})$. The transverse diffusion constant then is predicted[18] to exactly follow eq 4 at large ρ_r^*, a general result for any choice of "external" and nonlocalized (hence *not* self-consistent) model for $D_{\parallel}^{(r)}$ in eq 3.

Finally, we have analyzed the dynamic localization transition sphere volume fraction, ϕ_c, and find it can be understood in a universal manner; see the SM[18] for detailed discussions including mathematical derivations. Briefly, for $\rho_r^* \rightarrow 0$ (where $\phi_c \rightarrow \phi_{c,0}$) and $\gamma \gg 1$, needle localization occurs at a critical volume fraction of an "effective object" of spherocylindrical geometry with volume $\sim R^2 L$; the latter can be interpreted as the volume of a needle surrounded by spheres in contact with it. The effect of nonzero rod concentration enters only via a multiplicative factor, $\phi_c/\phi_{c,0}$, which is entirely controlled by $\rho_r^*/(1+\gamma)$. At high aspect ratio the latter scales as $2R/d_{T,0}$ in the entangled regime, which characterizes the ability of spheres to "cap" the tube. Hence, dynamic localization in entangled rods is understood as an extreme consequence of the blocked reptation effect.

In summary, we have developed a microscopic theory for rod diffusion in a hard sphere matrix that captures both topological entanglements and rod−sphere excluded volume constraints in a unified framework. Many new and testable qualitative and quantitative predictions have been made. While experimental[6−10] and simulation[11,16] studies are emerging for flexible chain nanocomposites with effectively immobile spheres, to the best of our knowledge there are no measurements or simulations of the analogue for rigid needles that our present work addresses.[20] However, opportunities do exist for future experimental tests by measuring the diffusion of entangled rodlike biopolymers (e.g., actin, microtubules, fibrin)[2,23] in crowded intracellular environments where obstacles can be effectively immobile[23] and also diffusion in quenched porous media[24] or holographically fabricated arrays of static mesoscopic particles.[25] Very specific simulation tests are definitely possible. More broadly, the present work provides a foundation for treating the diffusion of flexible chains in polymer nanocomposites,[6−11,16] perhaps by building on our "renormalized reptation" idea for entangled chains and primitive path and mapping ideas[15] for unentangled polymers. Finally, the approach can extended to treat both the effects of nonrandom composite structure and sphere mobility on tube localization and polymer diffusion.

■ ASSOCIATED CONTENT

Supporting Information

The most essential steps to derive eqs 1−4. Also included is a detailed analysis of the dynamic localization transition sphere volume fraction and the construction of a master plot. This material is available free of charge via the Internet at http://pubs.acs.org.

■ AUTHOR INFORMATION

Corresponding Author

*E-mail: kschweiz@illinois.edu.

Present Address

∥Division of Chemistry and Chemical Engineering, California Institute of Technology, Pasadena, CA.

Notes

The authors declare no competing financial interest.

■ ACKNOWLEDGMENTS

We acknowledge funding support from Michelin-France and stimulating discussions with Russ Composto.

■ REFERENCES

(1) McLeish, T. C. *Adv. Phys.* **2002**, *51*, 1379−1527.

(2) Wong, I. Y.; Gardel, M. L.; Reichman, D. R.; Weeks, E. R.; Valentine, M. T.; Bausch, A. R.; Weitz, D. A. *Phys. Rev. Lett.* **2004**, *92*, 178101. Gardel, M. L.; Kasza, K. E.; Brangwynne, C. P.; Liu, J.; Weitz, D. A. *Methods Cell Biol.* **2008**, *89*, 487−519.

(3) de Gennes, P. G. *J. Chem. Phys.* **1971**, *55*, 572−579.

(4) Doi, M.; Edwards, S. F. *The Theory of Polymer Dynamics*; Clarendon Press: Oxford, 1986.

(5) Zeng, Q. H.; Yu, A. B.; Lu, G. Q. *Prog. Polym. Sci.* **2008**, *33*, 191−269.

(6) Schneider, G. J.; Nusser, K.; Willner, L.; Falus, P.; Richter, D. *Macromolecules* **2011**, *44*, 5857−5860.

(7) Karatrantos, A.; Clarke, N.; Composto, R. J.; Winey, K. I. *Soft Matter* **2013**, *9*, 3877−3884.

(8) Gam, S.; Meth, J. S.; Zane, S. G.; Chi, C.; Wood, B. A.; Seitz, M. E.; Winey, K. I.; Clarke, N.; Composto, R. J. *Macromolecules* **2011**, *44*, 3494−3501; *Soft. Matter* **2012**, *8*, 6512−6520.

(9) Lin, C.; Gam, S.; Meth, J. S.; Clarke, N.; Winey, K. I.; Composto, R. J. *Macromolecules* **2013**, *46*, 4502−4509.
(10) Nusser, K.; Schneider, G. J.; Richter, D. *Soft Matter* **2011**, *7*, 7988−7991.
(11) Li, Y.; Kröger, M.; Liu, W. K. *Phys. Rev. Lett.* **2012**, *109*, 118001.
(12) Yamamoto, U.; Schweizer, K. S. *ACS Macro Lett.* **2013**, *2*, 955−959.
(13) Szamel, G. *Phys. Rev. Lett.* **1993**, *70*, 3744−3747. Szamel, G.; Schweizer, K. S. *J. Chem. Phys.* **1994**, *100*, 3127−3141.
(14) Sussman, D. M.; Schweizer, K. S. *Phys. Rev. Lett.* **2011**, *107*, 078102.
(15) Sussman, D. M.; Schweizer, K. S. *Phys. Rev. Lett.* **2012**, *109*, 168306.
(16) Li, Y.; Kröger, M.; Liu, W. K. *Soft Matter* **2014**, *10*, 1723−1737.
(17) Cichocki, B. *Z. Phys. B* **1987**, *66*, 537−540.
(18) See Supporting Information.
(19) Lamb, H. *Hydrodynamics*; Dover: New York, 1945.
(20) A few simulation studies have been conducted for the diffusion of a single rod (needle) in an array of static hard spheres or point scatters.[21,22] However, no direct comparison is presented since the previous work concerns 2-dimensional systems or Newtonian fluids rather than 3-dimensional Brownian systems. In addition, systematic understanding for rods or needles at nondilute concentrations have not been reported.
(21) Höfling, F.; Munk, T.; Frey, E.; Franosh, T. *Phys. Rev. E* **2008**, *77*, 060904.
(22) Tucker, A. K.; Hernandez, R. *J. Phys. Chem. B* **2011**, *115*, 4412−4418.
(23) Dix, J.; Verkman, A. *Annu. Rev. Biophys.* **2008**, *37*, 247−263.
(24) Chang, R.; Yethiraj, A. *J. Chem. Phys.* **2007**, *126*, 174906.
(25) Roichman, Y.; Grier, D. G.; Zaslavsky, G. *Phys. Rev. E* **2007**, *75*, 020401 (R).